Neutrino Scattering Results from CCFR

W. H. Smith, T. Kinnel, P. H. Sandler
University of Wisconsin, Madison, WI 53706

C. Arroyo, K. T. Bachmann, A. O. Bazarko, R. E. Blair, T. Bolton, C. Foudas, B. J. King, W. C. Lefmann, W. C. Leung, S. R. Mishra, E. Oltman, P. Z. Quintas, S. A. Rabinowitz, F. J. Sciulli, W. G. Seligman, M. H. Shaevitz
Columbia University, New York, NY 10027

F. S. Merritt, M. J. Oreglia, B. A. Schumm
University of Chicago, Chicago, IL 60637

R. H. Bernstein, F. O. Borcherding, H. E. Fisk, M. J. Lamm, W. Marsh, K. W. B. Merritt, H. Schellman, D. D. Yovanovitch
Fermilab, Batavia, IL 60510

A. Bodek, H. S. Budd, P. de Barbaro, W. K. Sakumoto
University of Rochester, Rochester, NY 14627

ABSTRACT

We present results from a high-statistics, high-energy neutrino-iron scattering experiment at the Fermilab Tevatron with 30 GeV $< E_\nu <$ 600 GeV. These include measurements of nucleon structure functions, $F_2(x, Q^2)$ and $xF_3(x, Q^2)$ from a sample of 1,320,000 ν_μ - and 280,000 $\overline{\nu}_\mu$ - induced charged current events and results from neutrino and antineutrino interactions with two muons in the final state measured using a sample of 220 $\mu^-\mu^-$ events, a sample of 25 $\mu^+\mu^+$ events and a sample of 5044 ν_μ and 1062 $\overline{\nu}_\mu$ induced $\mu^\mp\mu^\pm$ events. We also present the results of a preliminary determination of $\sin^2\theta_W$ from a study of 5×10^5 neutral current and charged current events with a mean neutrino energy of 166 GeV.

1 Introduction

We report on experimental studies of neutrino induced charged and neutral current interactions. We have studied 1.3 million neutrino-induced and 0.3 million antineutrino-induced charged current events with energies between 30 and 600 GeV to extract nucleon structure, study charm production, search for rare processes and measure the weak mixing angle. These are discussed in turn below.

1.1 Structure Functions

Neutrino scattering provides a unique technique for measuring both the F_2 and xF_3 structure functions which are associated, in the quark parton model, with the total quark $(q + \overline{q})$ and valence quark $(q - \overline{q})$ momentum, respectively. The predicted Q^2 evolution of xF_3 is particularly simple since it is not coupled to the unknown gluon distribution and, therefore, can be used as a unambiguous test of perturbative Quantum Chromodynamics and measurement of $\Lambda_{\overline{MS}}$. Combined analyses of F_2 and xF_3 allow the separation of the gluon evolution component and lead to information on the gluon structure function.

1.2 Dimuons

We next report on charged current interactions with two muons of the same and opposite electric charge in the final state. Events with two leptons of the same charge are expected to be mostly due to pion and kaon decay in the hadron showers of charged current events. Since the expected rate with respect to charged current events is less than one in 10,000 events, same sign dimuons offer the opportunity to test for the presence of new physics. Opposite sign events result from reactions that produce a charmed quark, followed by the leptonic decay of the charmed particle. Since charmed quarks are predominantly produced by valence down quarks and sea strange quarks, a measurement of the strange content of the nucleon can be extracted from the production rate and kinematics of the Opposite sign dimuon events. The strange quark structure function presented here is of particular theoretical interest in the exploration higher of order mass corrections [1], while the threshold behavior associated with the heavy charm mass is critical to the extraction of the weak mixing angle, $\sin^2\theta_W$ from neutrino neutral current data.

1.3 Weak Mixing Angle

Finally, we report a new measurement of $\sin^2\theta_W$. The Standard Model of Electroweak Physics requires as input five parameters to describe high-energy processes: α, G_F, M_Z, m_t, and m_h. The latter two enter into low-energy calculations, such as extracting $\sin^2\theta_W$ from νN scattering, via loop corrections to the W and Z self-energies. The radiative corrections to the effective $\sin^2\theta_W$'s measured in different interactions are quadratic in m_t for sufficiently large top mass, but only logarithmic in m_h. The strong dependence on the top mass, coupled with the LEP measurements of the Z^0 mass to an accuracy of 0.02% allows indirect determinations of m_t via precision measurements of neutral current νN scattering. Existing neutrino measurements of $\sin^2\theta_W$ already constrain the top mass to $m_t < 200$ GeV, a limit quite competitive with those attained by collider experiments[2]. Once the top mass is known, there is the possibility that sufficiently high precision measurements of $\sin^2\theta_W$ in different processes will constrain the Higgs mass or, perhaps through an inconsistency, point to new physics. Thus, considerable motivation exists to improve upon the determination of $\sin^2\theta_W$ in the neutrino sector[3].

1.4 Experiment

The neutrinos were provided by two runs in the Fermilab Tevatron neutrino Quadrupole-Triplet Beam (QTB). The QTB delivered $\overline{\nu}_\mu$ and ν_μ in the ratio of $\approx 1/2$, with energies from 30 to 600 GeV, at the CCFR detector[4]. We accumulated 3.7×10^6 charged-current triggers. The CCFR detector[5], consisted of a 690 ton iron-target calorimeter instrumented with liquid scintillation counters and drift chambers, followed by a 420 ton iron-toroid muon spectrometer. To ensure hadron shower containment and high track reconstruction efficiency, fiducial cuts were imposed upon the 3.7 million charged current triggers: a transverse event vertex within a square of 2.54m × 2.54m, a longitudinal event vertex at least 4.4m upstream of the downstream end of the target, and a selection on the muon track for charged current events to assure containment by the toroidal spectrometer.

2 Structure Function Measurement

The differential cross section for the ν-N charged-current process (CC), $\nu_\mu(\overline{\nu}) + N \rightarrow \mu^-(\mu^+) + X$, in terms of the Lorentz invariant structure functions F_2, $2xF_1$, and xF_3 is:

$$\frac{d\sigma^{\nu(\overline{\nu})}}{dxdy} = \frac{G_F^2 s}{2\pi}\left[\left(1 - y - \frac{Mxy}{2E_\nu}\right)F_2(x,Q^2) + \frac{y^2}{2}2xF_1(x,Q^2) \pm y(1-\frac{y}{2})xF_3(x,Q^2)\right]$$

where G_F is the weak Fermi coupling constant, M is the nucleon mass, E_ν is the incident neutrino energy, $s = 2E_\nu M + M^2$ is the ν-N center-of-mass energy, Q^2 is the square of the four-momentum transfer to the nucleon, the scaling variable $y = \frac{E_{HAD}}{E_\nu}$ is the fractional energy transferred to the hadronic vertex, and $x = \frac{Q^2}{2ME_\nu y}$, the Bjorken scaling variable, is the fractional momentum carried by the struck quark. The structure function $2xF_1$ is expressed in terms of F_2 and $R = \sigma_L/\sigma_T$, the ratio of total absorption cross sections for longitudinal and transverse polarized W bosons by $2xF_1(x,Q^2) = \frac{1+4M^2x^2}{1+R(x,Q^2)} \times F_2(x,Q^2)$. From the sums and differences of the differential cross sections of the ν-N and $\overline{\nu}$-N interactions, the "parity conserving" $F_2(x,Q^2)$ and the "parity violating" $xF_3(x,Q^2)$ structure functions are extracted. In the Quark-Parton Model (QPM), F_2 is the sum of all interacting nucleon constituents; and xF_3 is the difference of quark and anti-quark densities or the valence quark density of the nucleon.

2.1 Experimental Technique

To delineate only regions of high efficiency, two kinematic cuts, $E_\mu > 15$ GeV and $\theta_\mu < 0.150$ rad, were also imposed upon the reconstructed muons. After these selections, there remained a CC sample of 1,320,000 ν_μ – and 280,000 $\overline{\nu}_\mu$ – induced events, an increase by a factor of 11 (18) in $\nu_\mu(\overline{\nu}_\mu)$ event statistics, and a factor 2.5 increase in mean E_ν, over earlier CCFR Narrow Band Beam (NBB) samples[6].

Accurate measurements of structure functions in deep inelastic lepton experiments depend critically upon a good understanding of calibrations and energy resolutions. The CCFR detector was calibrated in two dedicated test runs, using charged particle beams of well defined momenta[4] the calibration studies detailed in Ref. [7], led to a systematic precision on E_{HAD} of about 1%, and on E_μ of about 0.5%.

No direct measurement of the neutrino flux was possible in the QTB. Absolute normalization of the flux, relevant for tests of the QPM sum rule predictions[8], was chosen so that the neutrino-nucleon total cross section equaled the world average of the isoscalar (Fe) target experiments, $\sigma^\nu = (.676 \pm .014) \times 10^{-38} cm^2 E_\nu$ (GeV)[9, 10]. The relative flux determination, *i.e.*, the ratio of fluxes among energies and between $\overline{\nu}$ and ν_μ, relevant for measurements of scaling violation and tests of Quantum Chromodynamics (QCD) predictions, was determined directly from the neutrino data using two techniques[10]. The extraction of F_2 and xF_3 is described in Ref. [10].

2.2 Mean Square Charge Test

The QPM relates the measurement of F_2 in ν-N scattering to those determined from the charged lepton, e-N or μ-N, scattering. The ratio of the two is a measure of the mean-square quark charge (in units of the square of the electron charge)[8]:

$$\frac{F_2^{lN}(x)}{F_2^{\nu N}(x)} = \frac{5}{18}\left(1 - \frac{3}{5}\frac{s+\overline{s}}{q+\overline{q}}\right). \qquad (1)$$

Here the small x-dependent correction in parentheses is due to the asymmetry of the strange and charm sea of the nucleon. The F_2^{lN} data were multiplied by (18/5) times the strange sea correction, and plotted in Fig. 1. The comparison of the CCFR-Fe data (solid circle) to those of SLAC-'D' (diamond)[15] BCDMS-'D' (square)[13], EMC-Fe (cross)[14], and CDHSW-Fe (fuzzy cross)[11] is shown in Fig. 1 in a few illustrative x-bins as a function of Q^2. For this comparison, the deuterium data were further corrected for the difference between the light and heavy nuclei using the measured ratio $F_2(Fe)/F_2(D)$ as a function of x[12]. This correction spanned a range from +4% at $x = 0.12$, to -4% at $x = 0.4$, to -12% at $x = 0.6$.

Figure 1 shows good agreement between the SLAC and the CCFR measurements of F_2. These are the first measurements showing substantial overlap with

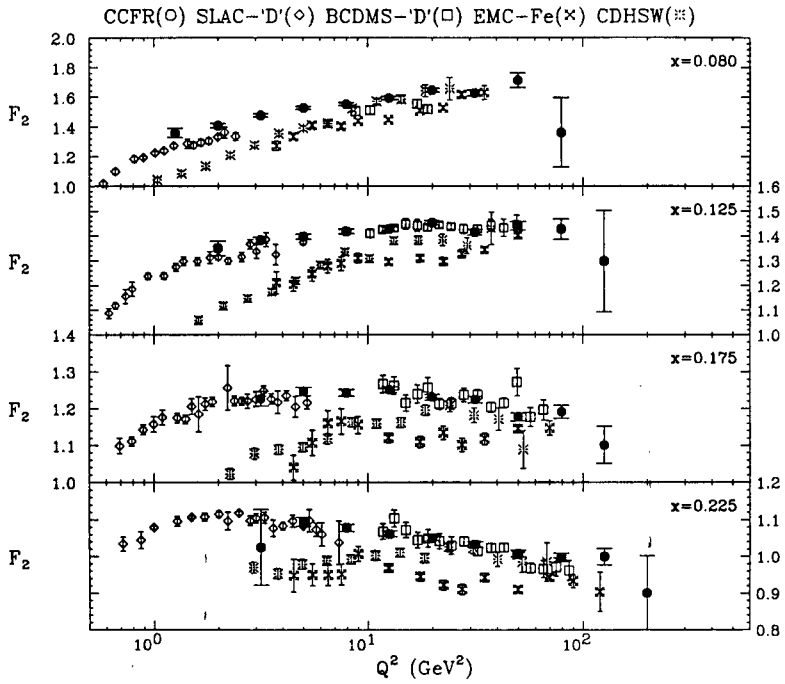

Figure 1: A comparison of $F_2(x, Q^2)$ as a function of Q^2, as measured by the CCFR, SLAC-'D', BCDMS-'D', EMC-Fe, and CDHSW-Fe in a few illustrative x-bins. The deuterium data have been corrected for the EMC-effect using the Fe/D measurement of SLAC. No arbitrary normalization factor is used.

the precise low-Q^2 SLAC data. At higher Q^2, the CCFR data are in good agreement with those of BCDMS-'D', and BCDMS-C data[13]; the latter, however, exist only in the limited range $0.25 \leq x \leq 0.80$, and for clarity are not shown in Fig. 1. The EMC-Fe data tend to be systematically lower in magnitude by about 7%; and a display steeper dependence on Q^2 at low x than those of CCFR.

The CDHSW data in the range $0.1 \leq x \leq 0.275$, tend to lie lower than those from this experiment, the disagreement being primarily in the low-Q^2 range of the x-bins. Although the extracted $F_2(x, Q^2)$ depend upon model dependent corrections which are not precisely the same in the two experiments, it should be noted that the corrections in the discrepant x-bins in Fig. 1 are no larger than ±2-4%. The origin of this x- and Q^2- dependent disagreement is not understood. The two data sets show better agreement for $x \leq 0.1$ and $x \geq 0.35$.

Data from each μ experiment are corrected using equation 1, and the muon-to-neutrino F_2 ratio is formed in each x-bin averaged over the overlapping Q^2 range with $Q^2 > 5$ GeV^2. It should be noted that the CCFR data which have a normalization error of ±2.5% span a larger range of any other single experiment. The BCDMS/CCFR average ratio (1.018±0.002±0.012±0.03 (norm) for BCDMS carbon and 1.000±0.002±0.012±0.03 for BCDMS "D") is in good agreement with the expected mean square charge. The EMC-Fe/CCFR ratios are systematically lower by about 7% than the prediction (average ratio is 0.921±0.002±0.023±0.05), but are reasonably constant as a function of x; although, due to the averaging over Q^2 the slope discrepancy would be obscured. The EMC-'D'/CCFR ratios show similar characteristics. The conclusions of this test do not change for a relaxed (> 1 GeV^2), or a more stringent (> 20 GeV^2) Q^2-cut.

2.3 QCD Analysis

We used a modified version of the Duke and Owens program to do a next-to-leading order QCD analysis with target mass correction. Applying cuts $Q^2 > 15$ GeV^2 to eliminate the non-perturbative region and $x < .7$ to remove the highest x-bin (where resolution corrections are sensitive to Fermi motion), best QCD fits to the data were obtained as illustrated in Fig. 2. The logarithmic slopes of the data agree well with the QCD prediction throughout the entire x-range. At low-x values the data agree well with predictions independent of the value of $\Lambda_{\overline{MS}}$. This is the first confirmation of the QCD prediction for scaling violations which is independent of assumptions about the gluon distributions and valid over the entire x range.

The value of $\Lambda_{\overline{MS}}$ resulting from the fit to xF_3 data was 179 ± 36 MeV, with a χ^2 of 53.5 for 53 degrees of freedom (χ^2=53.5/53). Varying the Q^2 cuts does not significantly change $\Lambda_{\overline{MS}}$; for $Q^2 > 10$ GeV^2, the best fit gives $\Lambda_{\overline{MS}} = 171 \pm 32$ MeV (χ^2=66.4/63); and for $Q^2 > 5$ GeV^2, $\Lambda_{\overline{MS}} = 170 \pm 31$ MeV (χ^2=83.8/80).

A more precise determination of $\Lambda_{\overline{MS}}$ from the non-singlet evolution is obtained by substituting F_2 for xF_3 at large values of x. The evolution of F_2 should conform

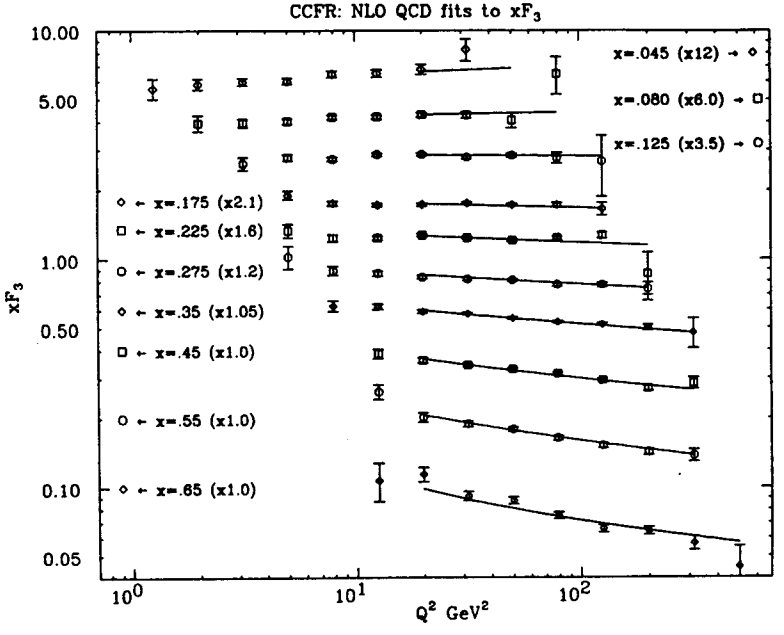

Figure 2: The xF_3 data and the best fit. Cuts of $Q^2 > 15$ GeV^2 and $x < 0.7$ were applied for a next-to-leading order fit including target mass corrections.

to that of a non-singlet structure function in a region, $x > x_{cut}$, so long as x_{cut} is large enough that the effects of antiquarks, gluons, and the longitudinal structure function are negligible on its Q^2 evolution. A conservative choice for x_{cut} is one beyond which the antiquarks are consistent with zero. For our best value of $\Lambda_{\overline{MS}}$ from non-singlet evolution we choose to substitute F_2 for xF_3 for $x > 0.5$. (The slopes for F_2 in this region are also shown in Fig. 3.) This non-singlet fit yields our best value:

$$\Lambda_{\overline{MS}} = 210 \pm 28 \text{ MeV for } Q^2 > 15 \text{ GeV}^2.$$

The data provide the first observation of the non-singlet structure function evolution consistent with QCD, and yield $\Lambda_{\overline{MS}} = 210 \pm 28 \pm 41$ MeV, where the second error is the systematic error, which is primarily due to the Hadron/Muon relative energy calibration uncertainty.

This four-flavor Next to Leading Order (NLO) value of $\Lambda^{(4)}_{\overline{\rm MS}} = 210 \pm 28$ (stat.) ± 41 (syst.) can be converted to a five flavor $\Lambda^{(5)}_{\overline{\rm MS}} = 140 \pm 21 \pm 30$. These values of Λ yield the following values of the strong coupling constant α_s for various values of Q^2.

At $Q^2 = 5$ GeV^2, α_s(NLO) $= .245 \pm .014 \pm .017$.
At $Q^2 = 25$ GeV^2, α_s(NLO) $= .190 \pm .007 \pm .010$.
At $Q^2 = M_z^2$, α_s(NLO) $= .111 \pm .002 \pm .003 \pm 0.03$ (scale).

2.4 GLS Sum Rule

The Gross-Llewellyn Smith (GLS) Sum Rule predicts that the integral of xF_3, weighted by $1/x$, equals the number of valence quarks inside a nucleon — three in the naive quark parton model. With next to leading order QCD corrections, the GLS sum rule can be written as

$$S_{GLS} \equiv \int_0^1 \frac{dx}{x} xF_3(x,Q^2) = 3\left[1 - \frac{12}{(33-2N_f)ln(Q^2/\Lambda^2)} + \mathcal{O}(Q^{-2})\right], \qquad (2)$$

where N_f is the number of quark flavor (=4) and Λ is the mass parameter of QCD. Higher twist effects, of the order $\mathcal{O}(Q^{-2})$, are expected to be small ($< 1\%$ of S_{GLS} at $x \approx 0.01$). The factor of 18 increase in the $\overline{\nu}$-induced charged current (CC) sample of the new data, compared to our earlier experiment, provides the most precise determination of xF_3, and an improved measurement of S_{GLS}.

To measure S_{GLS}, the values of xF_3 were interpolated or extrapolated to $Q_0^2 = 3$ GeV^2, which is approximately the mean Q^2 of the data in the x-bin which contributes most heavily to the integral. The resulting xF_3 is then fit to a function of the form: $f(x) = Ax^b(1-x)^c$ ($b > 0$). The best fit values are $A = 5.976 \pm 0.148$, $b = 0.766 \pm 0.010$, and $c = 3.101 \pm 0.036$. The integral of the fit weighted by $1/x$ gives the S_{GLS}. Figure 4 shows the measured $xF_3(x)$ at $Q^2 = 3$ GeV^2, as a function of x, the fits and their integrals. The measurement of the sum rule yields: $S_{GLS} = \int_x^1 \frac{xF_3}{x} dx = 2.50 \pm 0.018$(stat.) ± 0.078(syst.). The theoretical

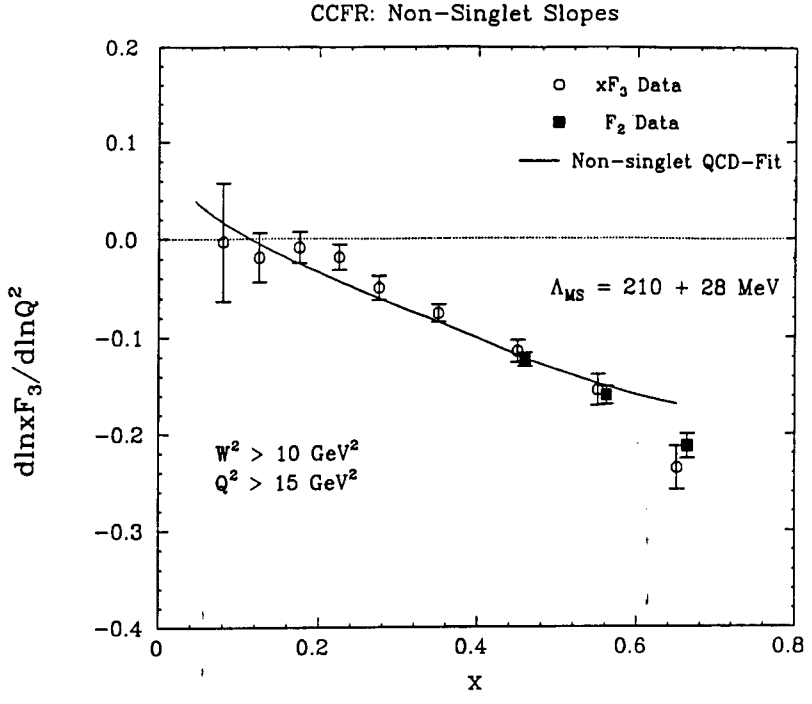

Figure 3: The slopes of xF_3 ($= \frac{d\ln xF_3}{d\ln Q^2}$) for the CCFR data are shown in circles. The curve is a prediction from perturbative QCD with target mass correction. The slopes for F_2 (squares) in the region $x > 0.4$ are also shown (with x values shifted by +2% for clarity).

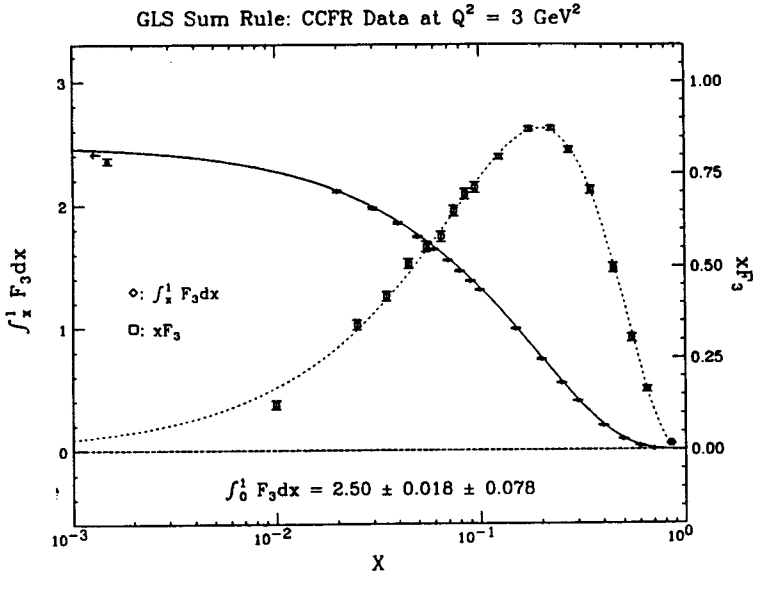

Figure 4: The GLS sum rule; the squares are $xF_3(x, Q^2 = 3)$ and the dashed line is the fit to $xF_3(x, Q^2 = 3)$ by $Ax^b(1-x)^c$. The solid line is the integral of the fit, $\int_x^1 \frac{dx}{x} xF_3$. The diamonds are an approximation to the integral computed by a weighted sum $[S(x_j)]$ of $xF_3^i = xF_3(x_i, Q^2 = 3)$, *i.e.*, $S(x_j) = \sum_j^n \delta x_i xF_3^i$.

prediction of S_{GLS}, for the measured $\Lambda = 210 \pm 50$ MeV from the evolution of the non-singlet structure function, is 2.66 ± 0.04. The prediction assumes negligible contributions from higher twist effects, target mass corrections, and higher order QCD corrections. A next-to-NLO calculation predicts $S_{GLS} = 2.63 \pm 0.04$.

3 Dimuons

Single muon and dimuon events were selected from the sample of charged-current triggers if they passed conditions ensuring proper reconstruction in the detector. To ensure that the muon did not exit the side of the detector before reaching the spectrometer, the angle of the muon at the vertex was required to be less than 250 mr with respect to the incident neutrino direction. In addition, the momentum of the muon was required to be at least 3 GeV/c at the front face of the muon spectrometer and 9 GeV/c at the event vertex, when corrected for energy loss in the target. The time of the track, determined from the drift chambers in the muon spectrometer, was required to be within 36 ns of the time obtained from the calorimeter counters and triggering toroid hodoscopes. About 1.5 million ν_μ and 0.3 million $\overline{\nu_\mu}$ induced charged-current events passed these selection criteria.

15000 candidate multimuon events were selected using two independent criteria based on calorimeter counter pulse heights downstream of the end of the hadron shower and indications of two tracks in the calorimeter drift chambers. The efficiency of this initial selection was 99%[16]. Pictures of the candidate events were scanned and about 4% of them were fixed interactively by physicists for errors in track reconstruction. This was a minor effect since 99% of the final sample of same-sign dimuons in E744 were found without interactively refitting the tracks[18].

3.1 Same-Sign Dimuons

Sources of prompt same-sign dimuons may include second-order quantum chromodynamic processes such as $c\bar{c}$ gluon bremsstrahlung and $D^0 - \overline{D^0}$ mixing. Non-prompt same-sign dimuons are produced by decaying pions or kaons in the hadron shower of a charged-current event. Since prompt sources cannot be distinguished from non-prompt sources in our apparatus, the non-prompt meson decay background must be subtracted from the observed number of same-sign dimuons to obtain the rate of prompt same-sign dimuon production. The rate of prompt same-sign dimuon production at energies below 200 GeV was measured by previous neutrino experiments to be somewhat higher than expected from theoretical predictions[19–25]. These measurements also seemed to indicate an increase in the prompt rate with increasing neutrino energy. However, in Fermilab experiment E744, the CCFR collaboration reported results with neutrino energies up to 600 GeV that were consistent with Standard Model predictions and with zero[16]. These measurements did not exhibit a strong energy dependence.

The results presented here are based on data from E744 and from an additional experiment with the same detector and beam, E770, such that the E744 statistics were more than doubled. In addition, we have made new improved measurements of non-prompt muon-production which lead to a substantial reduction in the systematic errors in the background calculation[28].

3.1.1 Event Selection

Same-sign dimuon events were selected from the candidate multimuon events with two tracks that passed the muon-track cuts described above. To ensure that the muons originate from the same incident neutrino, the transverse separation between the two tracks at the point of closest approach was required to be less than 15 cm. In addition, their time difference as determined from the tracks in the toroid gaps was required to be less than 28 ns. If there was third track with muon momentum at the vertex greater than 3.1 GeV/c, the event was identified as a trimuon and eliminated from the dimuon sample. The number of trimuons misidentified as dimuons was a background that was calculated as described below. Of the 1.8 million charged-current events, there were 220 $\mu^-\mu^-$ and 25 $\mu^+\mu^+$ events with $P_\mu > 9$ GeV/c. The non-prompt background is separated into two categories called the primary decay background and the secondary decay background. The primary decay background comes from events in which one of the primary hadrons at the hadron vertex decays to produce the second muon. The secondary decay background comes from events in which a secondary hadron a hadron produced in the subsequent interactions of the primary hadrons decays to produce the second muon.

3.1.2 Background Calculation

The calculation of the non-prompt background is taken from experimental data. The neutrino charged-current cross section is taken from the most recent CCFR structure functions[41]. The probability of a primary decay is given by parametrizations of a Monte Carlo calculation that is based on electroweak fragmentation measurements by neutrino bubble chamber experiments and well known interaction and decay probabilities[48]. The probability of a secondary decay is given by parametrizations of a Monte Carlo calculation based on newly measured muon-production rates in hadron-induced showers by the CCFR collaboration[30].

The 10% systematic uncertainty of the shower simulation is determined by its agreement with the test beam measurements used to set the level of muon-production in the simulation and the accuracy of the measurements. The total systematic uncertainty in the secondary decay background is 14.8% for incident neutrinos and 21.2% for incident antineutrinos. This includes the error from the input spectrum of primary hadrons: 10.9% for incident neutrinos and 18.7% for incident antineutrinos. There is an additional 10% error from the shower simulation and a 2% uncertainty from the interaction lengths of hadrons.

Neutrino production of trimuons becomes a background to same-sign dimuon production when the Opposite sign muon is hidden in the hadron shower. In order to be identified in the CCFR detector, the least energetic muon must traverse at least 2 m of steel, corresponding to an energy loss of 3.1 GeV. Hadronic trimuon production was modeled using the measured spectrum of hadronically produced muon pairs from experiments observing $\pi^+ Be \rightarrow \mu^+\mu^- X$[31]. The level and spectrum of trimuons due to radiative muon pair production was based on well understood theoretical calculations[32]. The level of hadronic trimuon production in the Monte Carlo was normalized to a corresponding sample of 86 trimuons observed in the CCFR detector, with the requirement that the momentum of the least energetic muon be greater than 4.5 GeV/c[33]. The calculated number of trimuons incorrectly identified as same-sign dimuons was 8.66 ± 5.54 $\mu^-\mu^-$ events and 1.02 ± 0.65 $\mu^+\mu^+$ events.

There is an additional background due to two charged-current events that come from the same RF bucket, which are produced by a neutrino in the same position within the detector. Such events are called overlays. Most are eliminated with the cuts described above on the time of passage of the muon tracks relative to the trigger time and on the transverse distance of closest approach. The overlay background was 1.10 ± 0.44 $\mu^-\mu^-$ events and 0.06 ± 0.03 $\mu^+\mu^+$ events[28].

The meson decay background comprises 94% of the total background, contributing 56.32 ± 8.35 $\mu^-\mu^-$ and 3.75 ± 0.80 $\mu^+\mu^+$ events from secondary decays, and 109.45 ± 11.95 $\mu^-\mu^-$ and 12.04 ± 2.25 $\mu^+\mu^+$ events from primary decays. The trimuon background comprises about 4% of the background, and the overlay background accounts for less than 1% of the background. The 220 $\mu^-\mu^-$ events have a total background from meson decays, misidentified trimuons, and overlays of 175.54 ± 19.35 events, while the 25 $\mu^+\mu^+$ events have a total background of 16.87 ± 3.04 events. This yields an observed prompt excess of 44.46 ± 24.38 $\mu^-\mu^-$ events and 8.14 ± 5.17 $\mu^+\mu^+$ events, where the error is statistical and systematic combined. The shapes of the kinematic distributions for the same-sign dimuon data and the meson-decay background are reasonably consistent[29].

3.1.3 Rates and Comparisons

The final rates for visible energies between 30 GeV and 600 GeV and $P_\mu > 9$ GeV/c are $(5.4 \pm 2.3) \times 10^{-5}$ or less than 9.2×10^{-5} at the 90% C.L. per charged-current event for incident ν_μ, and $(5.2 \pm 3.3) \times 10^{-5}$ or less than 10.5×10^{-5} at the 90% C.L. per charged-current event for incident $\overline{\nu_\mu}$. The errors include statistical and systematic uncertainties.

Figure 5 shows the rate due to the meson-decay background, which was multiplied by 0.4 to bring it down to the level of the data excess for shape comparison. The shape of the energy dependence for the meson-decay background agrees with the data. To ensure that no other sources of same-sign dimuons contribute to this excess, we calculated the expected rate due to prompt processes predicted by the Standard Model. For example, the range of rates expected from a $c\bar{c}$ gluon

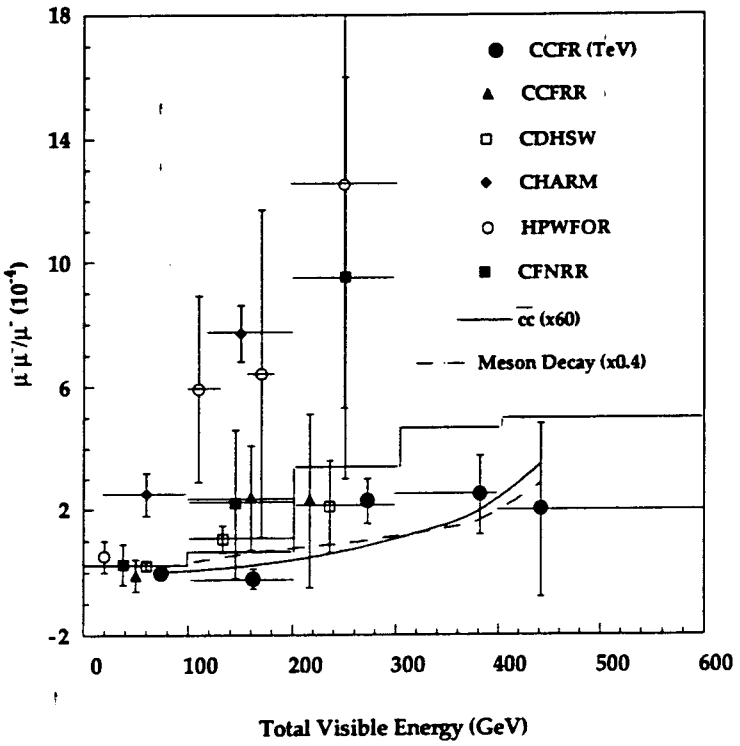

Figure 5: The prompt same-sign dimuon rates relative to the charged-current rate compared to previous experiments. The CCFR TeV points and the histogram representing the 90% C.L. upper limit are from this experiment. The dashed line represents the energy dependence of the meson-decay background rate, decreased by 0.4 to match the level of the same-sign dimuon data excess. The solid line represents the rate due to $c\bar{c}$ gluon bremsstrahlung increased by a factor of 60 to equal the level of the same sign excess.

Table 1: Comparison of prompt same-sign dimuon rates for several experiments for neutrino energies less than 300 GeV. The beam nomenclature is: NBB for narrow band beam, WBB for wide band horn focussed beam, QTB for quadrupole triplet beam.

Experiment	Reference	Beam Type	P_μ cut (GeV/c)	$\mu^-\mu^-/\mu^-$ $\times 10^{-4}$
CCFR	this expt.	QTB	9.0	0.36 ± 0.21
CCFR	[16]	QTB	9.0	0.24 ± 0.41
CCFRR	[19]	NBB	9.0	1.0 ± 0.7
CDHS	[20]	WBB	6.5	0.43 ± 0.23
CDHSW	[22]	NBB,WBB	9.0	1.16 ± 0.42
CHARM	[23]	WBB	4.0	4.5 ± 1.6
HPWFOR	[24]	QTB	10.0	3.0 ± 0.8
CFNRR	[25]	QTB	9.0	2.0 ± 1.1

bremsstrahlung calculation – based on the work of Barger et al.[34] and Cudell et al.[17] – is shown in Fig. 5. For this calculation, we set the mass of the charm quark parameter, m_c, to 1.3 ± 0.3 GeV/c^2, as recently measured by the CCFR collaboration in Opposite sign dimuon production[35]. The structure functions are the CCFR QTB structure functions[41] and the fragmentation of the c- quark to a D-meson is modeled with the Peterson fragmentation function[36]. The calculated $c\bar{c}$ gluon bremsstrahlung rate of same-sign dimuons with $P_\mu > 9$ GeV/c for the energies of this experiment is $(0.09 \pm 0.39) \times 10^{-5}$ per charged-current event for incident ν_μ or less than 0.7×10^{-5} at the 90% C.L. The error is composed of a factor of four due to the uncertainty in m_c and a factor of 1.2 due to the uncertainty on ϵ in the Peterson fragmentation function[37]. In addition, there is a factor of 30% due to the error on the strong coupling constant resulting from the experimental error on $\Lambda_{\overline{MS}}$ as determined by the evolution of non-singlet structure functions from the CCFR data[41]. The calculated $c\bar{c}$ gluon bremsstrahlung rate of $(0.09 \pm 0.39) \times 10^{-5}$ is too small to be considered an important contribution to the measured rate of prompt same-sign dimuon production.

A comparison of our results with the prompt ν_μ-induced same-sign rates from other experiments is shown in Table 1 for visible energies less than 300 GeV, while the energy dependence is given in Fig. 5. Note that the comparison of rates as a function of energy for different kinds of neutrino beams is uncertain. This is because the visible energy for same-sign events is smaller than the visible energy for charged-current events, and the energy distribution of the neutrino beam differs for QTB, wide-band, and narrow-band beams. This has not been accounted for in the comparison of Fig. 5.

The new CCFR rates do not show the energy dependence suggested by some

of the measurements prior to 1988. However, they agree with results reported previously by the CCFR collaboration[16] in 1988. The CFNRR experiment – the first high-density detector to measure a same-sign dimuon rate – initially reported a higher rate than expected from Standard Model calculations[25]. They subsequently revised their number, which agrees with our results[26]. The CHARM collaboration measured ν_μ induced same-sign dimuon rates at the CERN Super Proton Synchrotron (SPS) horn focussed beam[23]. For total energies between 100 GeV and 200 GeV, they measured a prompt rate of $(7.8 \pm 1.8) \times 10^{-4}$ per charged-current event. This measurement has the largest excess after background subtraction. Our rate for the same incident energies is $(-0.22 \pm 0.32) \times 10^{-4}$. Although, their muon momentum cut was 4 GeV/c, and ours was 9 GeV/c, there are important differences in the technique of background calculation. The CHARM collaboration determined the background directly from the spatial separation of the muon tracks at the event vertex, using the distribution of punchthrough hadrons as a measure of this quantity for the background. However, punchthrough hadrons are predominantly the secondary, not the primary hadrons that cause a majority of the meson decay background. Since secondary hadrons have a wider spatial distribution, their use would tend to underestimate the background.

The CDHSW experiment measured a prompt rate of $(1.16 \pm 0.42) \times 10^{-4}$ per charged-current event for neutrino energies between 100 GeV and 200 GeV with $P_\mu > 9$ GeV/c at the CERN SPS[22]. Based on 367 same-sign events, this is the most significant rate measured for energies less than 200 GeV. Our result of $(2.05 \pm 0.80) \times 10^{-4}$ for this energy bin is consistent with their measurement. Recently, the experiment E632 published results on same-sign dimuons measured with the Fermilab 15-ft bubble chamber in a QTB neutrino beam[27]. This beam was produced at the Tevatron so the neutrinos ranged between 30 and 600 GeV in energy. They observed 11 ν_μ-induced same-sign events to yield a limit of 1.1×10^{-3} at the 90% C.L. This is consistent with our 90% C.L. limit over the same neutrino energies of 9.2×10^{-5}. In general, the experiments that have the greater differences with the results presented here did not have sufficient access to precision measurements of muon-production rates in hadronic showers in order to accurately calculate the meson-decay background. A more detailed discussion of previous experiments can be found in Ref.[28].

3.2 Opposite sign Dimuons

Charged current neutrino-nucleon scattering involving an interaction with an s or d quark may produce a charm quark, which fragments into a charmed hadron and produces a second muon, of Opposite sign, through semileptonic decay. The heavy charm quark is expected to introduce an energy threshold in the dimuon production rate. This effect is described through the slow rescaling model[38], in which ξ, the momentum fraction carried by the struck quark, is related to the kinematic variable $x = Q^2/2ME_\nu y$ by the expression $\xi = x(1 + m_c^2/Q^2)$. Representing the momentum distribution of the s and d quarks within the nucleon as $s(\xi)$ and $d(\xi)$, the cross section for neutrino production of Opposite sign dimuons from charm may be written:

$$\frac{d^2\sigma(\nu N \rightarrow \mu^-\mu^+ X)}{d\xi\, dy} = \frac{G^2 M E_\nu}{\pi} \left\{ \xi d(\xi) |V_{cd}|^2 + 2\xi s(\xi) |V_{cs}|^2 \right\} \times [1 - \frac{m_c^2}{2ME_\nu \xi}] D(z) B_c$$

where the function $D(z)$ describes the fragmentation of charm quarks into charmed hadrons and B_c is the semileptonic branching ratio for charmed hadrons. The analogous equation for antineutrinos is found by substituting $d(\xi) \rightarrow \overline{d}(\xi)$ and $s(\xi) \rightarrow \overline{s}(\xi)$.

Previously published results from E744[39] described Opposite sign dimuon data for $30 \leq E_\nu \leq 600$ GeV with $P_\mu \geq 9$ Gev/c and $\theta_\mu \leq 250$ mrad demanded for both muon tracks. By combining the two samples, requiring $E_{had} \geq 10$ GeV, and lowering the $P_{\mu 2}$ cut to 5 GeV/c for $E_{had} \leq 130$ GeV, a sample of 5044 ν_μ 1062 $\overline{\nu}_\mu$ induced $\mu^\mp \mu^\pm$ events are observed, a more than threefold statistical enhancement. Muonic decays of non-prompt π and K mesons comprise the primary dimuon background of 796.5 ± 11.5 ν_μ and $118.0 \pm 2.1 \overline{\nu}_\mu$ events to the above sample[40].

3.2.1 Measurements of Parameters

Single and dimuon events were simulated using Monte Carlo techniques. Quark and antiquark momentum densities were obtained from the CCFR structure functions[41] using a modified Buras-Gaemers parameterization[42]. The strange quark x dependence is assumed to be given by $s(x) \propto (1-x)^\beta$ with the magnitude set by the parameter $\kappa = 2S/(\overline{U} + \overline{D})$ (where $S = \int_0^1 xs(x)dx$, etc.). The normalization is set by the ratio of data to Monte Carlo for the charged-current single muon events.

A multiparameter χ^2 minimization is used to compare the data and Monte Carlo events binned in five E_{vis} $(= E_{\mu_1} + E_{\mu_2} + E_{had})$ bins and ten x_{vis} $(= Q^2_{vis}/2M(E_{had} + E_{\mu_2}))$ bins. The Monte Carlo event weights are shifted by varying m_c, β, κ, and B_c, to minimize χ^2, yielding best values for the parameters and their errors.

3.2.2 Results

The largest source of systematic uncertainty is the charm fragmentation, modeled using the Peterson function[43] $D(z)$. The Monte Carlo is fit to the data for various fixed values of ϵ, and a study of the distribution of $Z_{vis} = E_{\mu_2}/(E_{\mu_2} + E_{had})$ permits a measurement of $\epsilon = .22 \pm .05$. This value is combined with the E531 emulsion result[44] (analyzed for $W^2 > 30$ GeV^2) of $\epsilon = .18 \pm .06$ to yield a neutrino average $\epsilon = .20 \pm .04$. This value is consistent with that from the ARGUS[45] and CLEO[46] e^+e^- experiments, which find $\epsilon = .19 \pm .03$ and $.156 \pm .015$ respectively. The uncertainty in ϵ is included directly in the fitting procedure through an additional term in the overall χ^2.

Other systematic errors are found by varying parameters within their uncertainties. These include: π/K background, the relative P_μ and E_{had} energy scale, dimuon data selection, R, and the u_v/d_v ratio [47]. Assuming the Particle Data Group values[48] of $|V_{cd}|^2 = .0484$ and $|V_{cs}|^2 = .9494$, the multiparameter fit yields:

$$m_c = 1.31^{+0.20+0.12}_{-0.22-0.11}\ GeV/c^2 \qquad \kappa = .373^{+.048+.014}_{-.041-.013} \tag{3}$$

$$\beta = 9.25^{+0.60+0.36}_{-0.55-0.25} \qquad B_c = 0.105 \pm .0066 \pm .0038 \tag{4}$$

where the first error is statistical and the second is systematic. The χ^2 of 42.5 for 46 degrees of freedom suggests excellent agreement between the data and Monte Carlo.

The difference between the strange sea exponent, β, and that of the total sea, $\alpha = 6.75$ (at $Q^2 = 18.08$), where $x\overline{q}(x) \propto (1-x)^\alpha$, provides a quantitative indication that the strange sea is softer than the $\overline{u}$ and $\overline{d}$ sea.

The value of κ in (2) is lower than previous CCFR results[8, 48]. This is due to an increase in the non-strange sea for the latest measured structure functions[41]. Defining the strange sea content of the nucleon as $\eta_s = 2S/(U+D)$, the measured value of κ and $R = \overline{Q}/Q = .195$ at $Q^2 = 18.08\ GeV^2/c^2$ combine to yield:

$$\eta_s = 0.064^{+.0072}_{-.0062} \pm .0020.$$

This result is consistent with η_s from the previous publications.

Figure 6 shows the energy dependence of the ratio of dimuon to single muon production. The ratio of dimuon to single muon production serves as a direct test of the slow rescaling hypothesis. The acceptance corrected rates exhibit an energy dependence characteristic of heavy charm quark production. Once corrected for this threshold with $m_c = 1.31$ the rates flatten out, exhibiting only the sharp, low energy threshold behavior associated with the production of heavy charmed mesons as shown in Fig. 6.

The strange quark momentum distributions $xs(x)$ are found from the observed dimuon event distributions, corrected for acceptance and charm mass effects using the slow rescaling model. Figure 7 shows the Q^2 variations in $xs(x)$ for each value of x. The strange sea structure functions demonstrate scaling violations analogous to those seen in non-strange quarks[41].

If the CKM matrix elements are not assumed then the results of the fits in Eqs. (3) and (4) can be rewritten in terms of the products:

$$|V_{cd}|^2 B_c = 5.09 \pm .32^{+.17}_{-.16} \times 10^{-3}.$$

Substitution of the neutrino world average charm branching ratio[49] $B_c = .116 \pm .010$ yields:

$$|V_{cd}| = .209 \pm .011 \pm .0035.$$

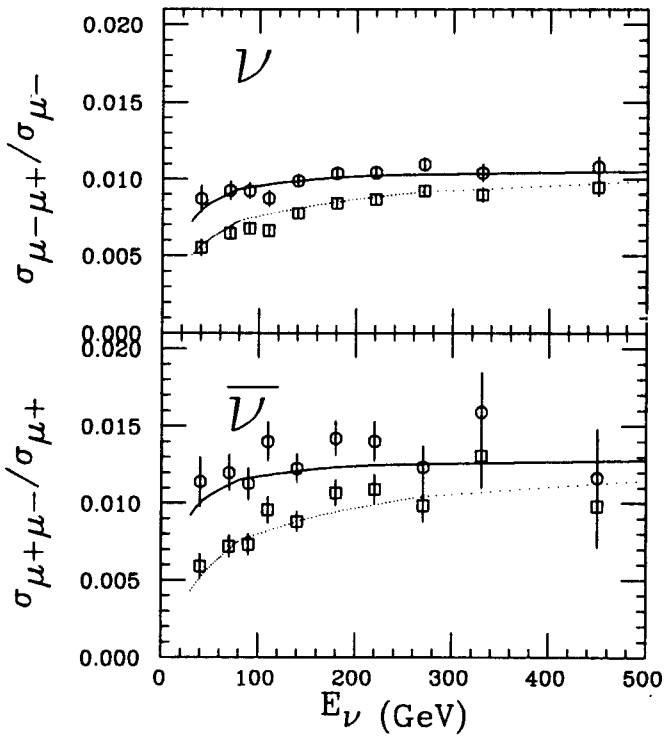

Figure 6: Opposite-sign dimuon rates versus E_ν for ν_μ (top) and $\overline{\nu}_\mu$ (bottom) data. Rates corrected for acceptance, smearing, and kinematic cuts are indicated by squares. Those corrected for slow rescaling with $m_c = 1.31$ are given by circles. The curves indicate the slow rescaling model prediction with $m_c = 1.31\ GeV/c^2$ (dotted) and $m_c = 0.0\ GeV/c^2$ (dashed).

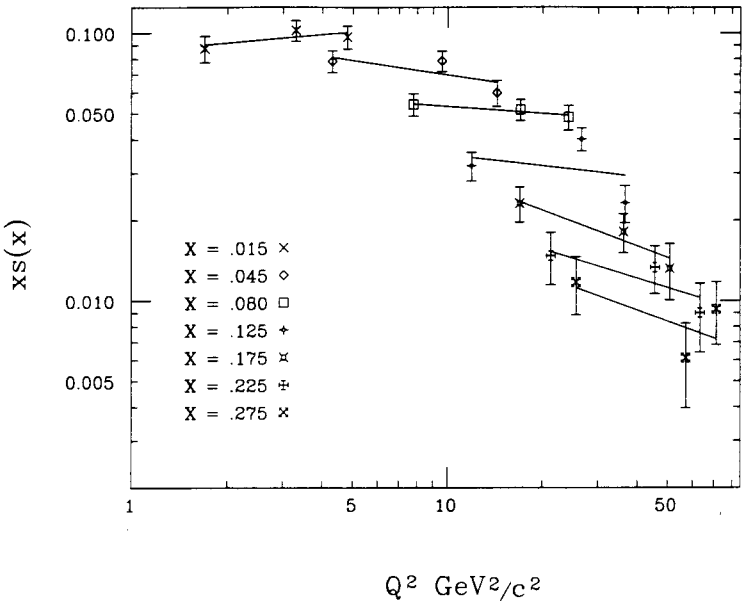

Figure 7: Strange sea structure functions $xs(x)$ versus Q^2 for several values of x. The lines are power-law fits to the data. Errors are statistical. An additional 11% scale error arises due to the uncertainty in κ.

4 Measurement of $\sin^2\theta_W$

Three essential quantities enter into the $\sin^2\theta_W$ analysis: the event length, the event radial vertex position, and the event energy. The length is defined as $L = place - cexit + 1$. *Place* is the most upstream of the first pair of two consecutive scintillation counters that each record at least four minimum ionizing particles (mips) equivalent energy; and *cexit* is the first counter upstream of the first occurrence of a gap of three consecutive counters each with energy less than 0.25 mip downstream of *place*. Note that $place = 1$ or $cexit = 1$ refers to the most downstream counter. We separate events into three categories based on L and *cexit*: *short* events with $L < 31$ counters (3 m of steel), which are mostly neutral current events; *toroid* events with $cexit < 3$, which are mostly charged current events exiting the calorimeter and entering the toroid; and *intermediate* events with $L > 30$ counters and $cexit > 3$, which are dominantly charged current events in which the muon exits the calorimeter or ranges out. To make this classification sensible, we require *place* to be at least 3.4 m of steel (34 counters) from the downstream end of the calorimeter and 0.6 m of steel (6 counters) from the upstream end.

The event transverse vertex position is obtained from a weighted sum of drift chamber hits from the first two drift chamber planes downstream of *place*. To minimize the number of charged current events with $L < 31$ which exit the sides of the detector and to suppress electron neutrino background, we require the event radius to be less than 76.2 cm. The event energy is defined as the sum of pulse heights from the first twenty counters in the event, starting with *place*. We require events to have at least 30 GeV of visible energy. This cut insures that the calorimeter is being used well within its linear regime, guarantees 100% trigger efficiency, and strongly suppresses non-deep-inelastic processes and the cosmic ray background. After all cuts, our event sample contains 1.51×10^5 short events, 2.93×10^5 toroid events, and 0.42×10^5 intermediate length events, with a mean neutrino energy of 166 GeV. This represents the highest energy high-statistics-neutral-current neutrino measurement to date.

4.1 Analysis Technique

To determine the weak mixing angle, we attempt to reproduce the measured ratio of *short* to *toroid* events, $R_{30} \equiv \frac{N_{short}}{N_{toroid}}$, with a Monte Carlo. The Monte Carlo includes as ingredients the QCD corrected quark-parton model, a parametrization of the quadrupole-triplet neutrino beam, and a detailed description of the Lab E detector. To first approximation, $R_{30} \simeq R_\nu$, where R_ν is the ratio of neutral current to charged current cross sections. Previous $\sin^2\theta_W$ determinations consisted of extracting a suitably corrected value of R_ν and then applying the Llewellyn-Smith formalism[50]. We forego that approach here and instead attempt to adjust our Monte Carlo to match our data using $\sin^2\theta_W$ as the single free parameter.

The composition of short length events is approximately 60% ν_μ neutral current, 22% ν_μ charged current, 9% $\bar{\nu}_\mu$ neutral current, 1% $\bar{\nu}_\mu$ charged current, and 8% ν_e charged and neutral current.

The parton distributions in our Monte Carlo are obtained directly from structure function measurements by the same experiment[41]. Corrections must be made for the non-isoscalar target, QED radiative effects, the strange and charm sea of the nucleon, the longitudinal structure function, and charm production. The last is the most important. As detailed in Sec. 3.2 charm production is modeled via the slow rescaling formalism in which charm threshold effects are parametrized using an effective charm mass, m_c. The present $\sin^2\theta_W$ analysis uses a value of $m_c = 1.34 \pm 0.34$ GeV from a previous analysis of 6000 Opposite sign dimuon from this experiment[51].

4.2 Neutrino Flux

The dominant component of the neutrino flux arising from two-body charged pion and kaon decays is directly measured in the experiment. A more serious issue is the electron neutrino flux. Since all ν_e interactions produce short length events, a mis-estimate of this component of the flux translates into a large error on $\sin^2\theta_W$. There are two components to the ν_e flux. The first, originating from $K^+ \to \pi^0 e^+ \nu_e$, can be tightly constrained from $K_{\mu 2}$ decays, whose contribution from the flux can be separated from $\pi_{\mu 2}$ contribution by exploiting the well known energy-radius correlation. The second component of the ν_e flux is from $K_L^0 \to \pi^- e^+ \nu_e$; these decays contribute $\sim 17\%$ of the ν_e events. This source is important because the primary proton beam is targeted at 0 degrees relative to the Lab E detector to maximize total flux for charged current measurements. The K_L component cannot be constrained using $K_L^0 \to \pi^- \mu^+ \nu_\mu$ decays because the neutral $K_{\mu 3}$ decays are a small fraction of the charged $K_{\mu 2}$ decays. The K_L^0 component must instead be calculated using other experimental data on K_L^0 production[52].

A check on the ν_e flux calculation can be obtained from the data itself by exploiting the different longitudinal energy distribution of charged current ν_e events compared to ν_μ neutral current events. The quantity η_3 is defined as $\eta_3 = 1 - E_3/E_{tot}$, where E_3 is the sum of the energy in the three most upstream counters and E_{tot} is the total energy. Muon neutrino neutral current events are characterized by a broad distribution in η_3, reflecting the large fluctuations in hadronic shower length. Electron neutrino charged current events, by contrast, have an η_3 distribution that is peaked towards small values of η_3 since a substantial portion of the event energy is carried by an electron. It is possible to obtain the shape of the η_3 distribution for neutral current events empirically from charged current events in which the muon has been removed, and to obtain the electron neutrino shape by convolving hadron showers from charged current events with electron showers from a test beam. The two independent calculations are consistent to within the errors of $\pm 4.6\%$ for the flux Monte Carlo and $\pm 6.8\%$ for the η_3 fits. Combining the two results, the estimated uncertainty for the ν_e flux is $\pm 3.8\%$. This error is dominated by the 20% uncertainty in K_L^0 production of ν_e.

The critical detector parameters that must be modeled are the calorimeter response to hadrons, muons, and electrons; and the efficiency and noise characteristics of the counters with respect to minimum ionizing particles. The electron, pion, and muon calorimeter performance has been studied for energies from 8-400 GeV in test beam runs in 1984, 1987, and 1991; hence accurate parametrizations based on real data are available. Muon energy loss in the 20 counter energy definition region is particularly important as the presence of the muon generates an asymmetry in the charged current versus neutral current flux. Our muon energy loss parametrization is tuned with a large sample of "straight through" beam muons taken at the same time as the neutrino data. Noise and efficiency are measured counter-by-counter as a function of radial position using beam muons. The detector portion of the Monte Carlo is thus almost completely a parametrization of actual data. A small exception is the correction of the event longitudinal vertex for albedo effects. This correction is based on Geant/Gheisha[53]. However, we have been able to verify the Geant correction, on average, by comparing the event vertex determined from tracking information in dimuon events versus that obtained from the calorimeter.

4.3 Result

Our Monte Carlo predicts

$$\sin^2\theta_W - 0.230 = -1.525 \cdot (R_{30} - 0.5182)$$

for events satisfying our fiducial and energy cuts. The data give

$$R_{30} = 0.5151 \pm 0.0016_{stat},$$

implying an uncorrected value:

$$\sin^2\theta_W{}^{uncorr.} = 0.2338 \pm 0.0029_{stat} \quad \text{(preliminary)}.$$

The statistical error includes the contribution of Monte Carlo statistics and will in the near future be reduced to the data value of ± 0.0023. Figures 8 and 9 show the distributions of event length and visible energy for the data with Monte Carlo predictions overlaid. The agreement between data and Monte Carlo is good.

4.4 Corrections and Systematic Errors

Three non-Monte Carlo corrections have been made to $\sin^2\theta_W$ to give the final result:

1) A correction of $+0.0011$ to $\sin^2\theta_W$ due to cosmic rays. This correction has been measured using events taken out of time with the neutrino beam.

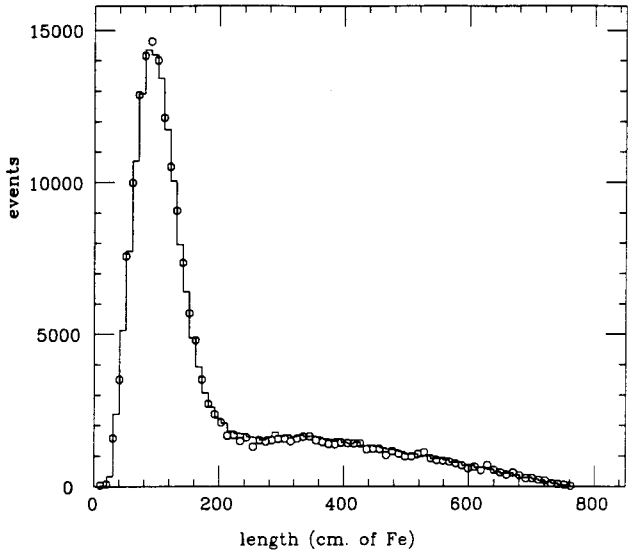

Figure 8: Event length for data (solid histogram) and Monte Carlo (plotted points) with $\sin^2\theta_W{}^{uncorr.} = 0.2338$.

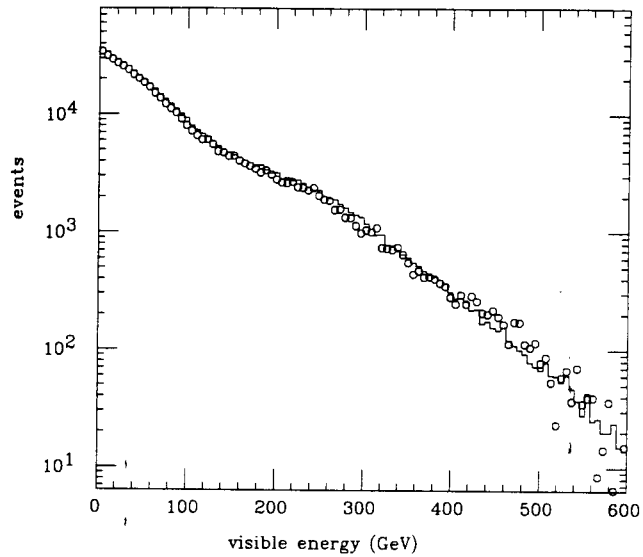

Figure 9: Visible energy distribution for data (solid histogram) and Monte Carlo (plotted points) with $\sin^2\theta_W{}^{uncorr.} = 0.2338$.

Table 2: Summary of present E770 errors on weak mixing angle.

SOURCE	ERROR
data statistics	0.0023
Monte Carlo statistics	0.0018
TOTAL STATISTICAL	0.0029
$\nu_\mu, \bar{\nu}_\mu$ flux	0.0010
energy scale, resolution	0.0009
length determination	0.0014
ν_e flux	0.0027
TOTAL EXP. SYSTEMATIC	0.0033
structure functions	0.0003
non-isoscalarity ($\delta\frac{U_V}{D_V} = \pm 10\%$)	0.0017
long. struct. func. ($\delta R_L = \pm 10\%$)	0.0014
charm mass ($\delta m_c = \pm 0.34 GeV$)	0.0034
strange sea ($\delta\kappa = \pm 0.07$)	0.0006
charm sea ($\delta\frac{c}{s} = 15\%$)	0.0019
higher twist	0.0005
radiative corrections	0.0010
TOTAL MODEL	0.0047

2) A correction of -0.0017 to take into account special kinematic properties of charm production associated di-lepton events in the charged current sector which are absent in neutral currents. An example is the presence of missing energy in events containing a charm quark which has decayed semi-leptonically.
3) A correction of -0.0085 to account for radiative corrections not taken into account in our Monte Carlo. Corrections due to muon bremsstrahlung are sensitive to our cuts and are thus explicitly taken into account via the formalism of De Rujula *et al.*[55]. The remaining correction is obtained from Sirlin and Marciano[54]. This radiative correction procedure has been checked against a calculation by Bardin[56]; the two methods agree to 0.001 in $\sin^2\theta_W$.

After applying the corrections, our preliminary value for $\sin^2\theta_W$ is

$$\sin^2\theta_W = 0.2242 \pm 0.0029_{stat} \pm 0.0033_{exp} \pm 0.0047_{model}.$$

Systematic errors are broken down in Table 2. The two most important for this experiment are those associated with charm production (± 0.0034) and the ν_e flux (± 0.0027). Combining the statistical and experimental systematics: $\sin^2\theta_W = 0.2242 \pm 0.0044 \pm 0.0047$. This can be compared with the two highest precision existing measurements, $\sin^2\theta_W = 0.228 \pm 0.005 \pm 0.005$ by CDHS[57] and $\sin^2\theta_W = 0.236 \pm 0.005 \pm 0.005$ by CHARM[58]. Our value is consistent with these two results, though slightly lower.

The largest model error is due to uncertainties in charm production in the charged current sector. While the magnitude of this systematic error is not much less than previous analysis, we feel this contribution is under much better control. The 30 GeV visible energy cut that we impose lessens the influence of the charm threshold. More importantly, we have measured all of the parameters of the slow rescaling model of charm production in the same experiment. Charm production is thus accurately parametrized for our experiment, independent of the theoretical validity of the charm production model. Final analysis of the dimuon data from this experiment should reduce the charm associated error by 25%. Because charm production is sensitive to details of the model, e.g., the sea quark distributions, and to experimental details like the neutrino energy spectrum, one is cautioned against simply substituting our charm mass and its error into other experimental analyses to obtain "better" values of $\sin^2\theta_W$. The slow rescaling model parameters used in this analysis accurately parametrize charm production in Fermilab E744/770. The largest experimental systematic uncertainty is from lack of knowledge of the ν_e flux, which is itself driven by the poorly constrained contribution of K^0_L decays to the ν_e flux.

5 Conclusions

Precision tests of QCD have been performed using the new CCFR high statistics neutrino data sample. These data, in conjunction with SLAC and BCDMS data, provide a consistent set of structure functions over a large range of Q^2. The data provide the first observation of the non-singlet structure function evolution consistent with QCD and yield a gluon independent value of $\Lambda^{(4)}_{\overline{MS}} = 210 \pm 28$ (stat.) ± 41 (syst.). We have also measured the Gross-Llewellyn Smith Sum Rule value of $S_{GLS} = 2.50 \pm 0.018$(stat.) ± 0.078(syst.), which is consistent with the expected value for three valence quarks of 2.66 ± 0.04.

We have increased the statistical significance of the total same-sign dimuon rate. Furthermore, detailed measurements of muon-production in hadron showers to calculate the secondary component of the meson-decay background reduced the systematic uncertainty in the rate of same-sign production. The rate of prompt same-sign dimuon production with $P_\mu > 9$ GeV/c in ν_μ-N interactions for incident energies between 30 GeV and 600 GeV is $(5.3 \pm 2.4) \times 10^{-5}$ per ν_μ charged-current event or less than 9.2×10^{-5} at the 90% C.L. For incident $\overline{\nu_\mu}$ the rate is $(5.2 \pm 3.3) \times 10^{-5}$ per charged-current event or less than 10.5×10^{-5} at the 90% C.L.

The Opposite sign dimuon data support the slow rescaling hypothesis for a value of $m_c = 1.31 \pm .24$. The charm mass error constitutes the single largest source of theoretical uncertainty in precision measurements of the weak mixing angle, $sin^2\theta_W$. The new result will reduce this uncertainty significantly, from .0034 to .0024. The CKM matrix element is found to be $|V_{cd}| = .209 \pm .012$. The nucleon strangeness content is measured to be $\eta_s = .064^{+.0075}_{-.0065}$ and the strange sea

is found to be softer than its non-strange counterpart. The measurement of the Q^2 dependence of the strange sea structure function $xs(x)$ may be used to test perturbative-evolution predictions and evaluate flavor asymmetry in the sea.

Finally, we have a new preliminary measurement of $\sin^2\theta_W = 0.2242 \pm 0.0044 \pm 0.0047$, which has a charm model error that is better understood due to the 30 GeV visible energy cut and the direct measurement of the charm threshold in the same experiment.

References

[1] M. A. Aivazis, F. I. Olness, and W. K. Tung, Fermilab Pub-90/23; V. Barone *et al.*, Phys. Lett. **B268**, 279 (1991).

[2] D. C. Kennedy and P. Langacker, Phys. Rev. **D44**, 1591 (1991); P. Langacker and M. Luo, Phys. Rev. **D44**, 817 (1991); P. Langacker, M. Luo, and A. Mann, Rev. Mod. Phys. **64**, 87 (1992).

[3] The weak mixing angle in extracted in neutrino scattering from the ratio of the charged current-to-neutral current cross sections is, due to a near cancellation of two corrections, nearly equal to the on-shell definition: ${\sin^2\theta_W}^{\nu} \simeq {\sin^2\theta_W}^{S} = 1 - M_W^2/M_Z^2$ to within ± 0.002 for top masses less than 230 GeV. W. J. Marciano and A. Sirlin, Phys. Rev. **D26**, 2695 (1980); R. G. Stuart, Z. Phys. **C34**, 445 (1987).

[4] W. K. Sakumoto *et al.*, Nucl. Inst. Meth. **A294**, 179 (1990); B. J. King *et al.*, Nucl. Inst. Meth. **A302**, 254 (1991).

[5] F. S. Merritt *et al.*, Nucl. Inst. Meth. **A245**, 27 (1986).

[6] D. B. MacFarlane *et al.*, Z. Phys. **C26**, 1 (1984); E. Oltman *et al.*, accepted for publication in Z. Phys. **C**.

[7] P. Z. Quintas *et al.*, Nevis Preprint # 1461; submitted to Phys. Rev. Lett. Also see P. Z. Quintas, Ph.D. Thesis, Columbia University, 1991.

[8] S. R. Mishra and F. Sciulli, Ann. Rev. Nucl. Part. Sci. **39**, 259 (1989).

[9] CCFR: R. E. Blair *et al.*, Phys. Rev. Lett. **51**, 343(1983); CDHSW: P. Berge *et al.*, Z. Phys. **C35**, 443 (1987); CCFR: P. Auchincloss *et al.*, Z. Phys. **C48**, 411 (1990).

[10] W. C. Leung *et al.*, Nevis Preprint # 1460; submitted to Phys. Rev. Lett. Also see W. C. Leung, Ph.D. Thesis, Columbia University, 1991.

[11] CDHSW: P. Berge *et al.*, Z. Phys. **C49**, 187 (1991).

[12] SLAC: A. Bodek *et al.*, Phys. Rev. Lett. **50**, 1431 (1983); **51**, 534 (1983).

[13] BCDMS: A. C. Benvenuti *et al.*, Phys. Lett. **B237**, 592 (1990) (D-target); A. C. Benvenuti *et al.*, Phys. Lett. **B195**, 91 (1987) (C-target).

[14] EMC: J. J. Aubert *et al.*, Nucl. Phys. **B272**, 158 (1986) (Fe Target); J. Ashman *et al.*, Phys. Lett. **B202**, 603 (1988) (D Target). The additional low-x deuterium data were obtained from S. J. Wimpenny.

[15] L. W. W. How, E. M. Riordan, S. Dasu, S. Rock, A. Bodek, SLAC-PUB-5422, to be published in Physics Letters **B** (1992).

[16] B. A. Schumm *et al.*, Phys. Rev. Lett. **60**, 1618 (1988).

[17] J. R. Cudell, F. Halzen, and K. Hikasa, Phys. Lett. **B175**, 227 (1986).

[18] B. A. Schumm, Ph.D. Thesis, University of Chicago, 1988.

[19] K. Lang *et al.*, Z. Phys. **C33**, 483 (1987).

[20] J. G. H. DeGroot *et al.*, Phys. Lett. **86B**, 103 (1979).

[21] M. Holder *et al.*, Phys. Lett. **70B**, 396 (1977).

[22] H. Burkhardt *et al.*, Z. Phys. **C31**, 39 (1985).

[23] M. Jonker *et al.*, Phys. Lett. **107B**, 241 (1981).

[24] T. Trinko *et al.*, Phys. Rev. **D23**, 1889 (1981).

[25] K. Nishikawa *et al.*, Phys. Rev. Lett. **46**, 1555 (1981).

[26] K. Nishikawa *et al.*, Phys. Rev. Lett. **54**, 1336 (1985).

[27] V. Jain *et al.*, Phys. Rev. **D41**, 2057 (1990).

[28] P. H. Sandler, Ph.D. Thesis, University of Wisconsin-Madison, 1992.

[29] P. H. Sandler *et al.*, submitted to Z. Phys. **C**, 1992.

[30] P. H. Sandler *et al.*, Phys. Rev. **D42**, 761 (1990).

[31] K. J. Anderson *et al.*, Phys. Rev. Lett. **37**, 799 (1976).

[32] V. Barger, T. Gottschalk, and R. J. N. Phillips, Phys. Rev. **D17**, 2284 (1977).

[33] This cut on the momentum of the least energetic muon for the identified trimuon events was chosen to minimize trimuons from meson-decays in the hadron shower of Opposite sign dimuon events.

[34] V. Barger, W. Y. Keung, R. J. N. Phillips, Phys. Rev. **D25**, 1803 (1982).

[35] M. H. Shaevitz, Nucl. Phys. **B19** (Proc. Suppl.), 270 (1991).

[36] C. Peterson *et al.*, Phys. Rev. **D27**, 105 (1983).

[37] H. Albrecht *et al.*, Phys. Lett. **105B**, 235 (1985).

[38] H. Georgi and H. D. Politzer, Phys. Rev. **D14**, 1829 (1976); R. M. Barnett, Phys. **D14**, 70 (1976).

[39] C. Foudas *et al.*, Phys. Rev. Lett. **64**, 1207 (1990).

[40] P. H. Sandler *et al.*, Wisconsin Preprint WISC-EX-92-324, submitted to Z. Phys. **C**.

[41] S. R. Mishra *et al.*, Nevis Preprint 1459, Dec. 1991, submitted to Phys. Rev. Lett.; W. C. Leung *et al.*, Nevis Report 1460, Dec. 1991, submitted to Phys. Rev. Lett.; P. Z. Quintas *et al.*, Nevis Report 1461, Dec. 1991, submitted to Phys. Rev. Lett.

[42] A. J. Buras, K. J. F. Gaemers, Nucl. Phys. **B132**, 249 (1978). At $Q^2 = 18.08$ the parton densities are given by $xu_v(x) = 2.718x^{0.61}(1-x)^{2.95}$, $xd_v(x) = 0.577xu_v(x)(1-x)$, and $sea(x) = 1.260(1-x)^{6.75}$.

[43] C. Peterson *et al.*, Phys. Rev. **D27**, 105 (1983).

[44] N. Ushida *et al.*, Phys. Lett. **B121**, 292 (1983).

[45] H. Albrecht *et al.*, Phys. Lett. **B150**, 235 (1985).

[46] D. Bortoletto *et al.*, Phys. Rev. **D37**, 1719 (1988).

[47] D. Allasia *et al.*, Phys. Lett. **B249**, 366 (1990).

[48] Review of Particle Properties, Phys. Lett. **B239** (1990).

[49] M. H. Shaevitz, Neutrino '90, Nucl. Phys. **B19** (Proc. Suppl.), 270 (1991).

[50] C. H. Llewellyn-Smith, Nucl. Phys. **B228**, 205 (1983).

[51] M. H. Shaevitz, Nucl. Phys. **B19** (proc. supp.), 270 (1991); S. A. Rabinowitz *et al.*, submitted to Phys. Rev. Lett.

[52] P. Skubic *et al.*, Phys. Rev. **D18**, 3115 (1978).

[53] R. Brun *et al.*, CERN-DD/78/2, 1978.

[54] A. Sirlin and W. J. Marciano, Nucl. Phys. **B189**, 442 (1982).

[55] A. De Rujula, R. Petronzio, and A. Savoy-Navarro, Nucl. Phys. **B154**, 394 (1979).

[56] D. Yu. Bardin and O. M. Fedorenko, Sov. J. Nucl. Phys. **30**, (1979) 418; and private communication.

[57] H. Abramowicz *et al.*, Phys. Rev. Lett. **57**, 298 (1986).

[58] J. V. Allaby *et al.*, Z. Phys. **C36**, 611 (1987).